

Journal of Biological Systems  
© World Scientific Publishing Company

## A Methodology for Tracking Solute Distribution in a Mathematical Model of the Kidney

Anita T. Layton

*Department of Mathematics, Duke University, Box 90320, Durham, North Carolina 27708, USA.*

*alayton@math.duke.edu*

*<http://www.math.duke.edu/faculty/alayton>*

Received (Day Month Year)

Revised (Day Month Year)

The goal of this study is to develop a methodology for tracking the distribution of filtered solute in mathematical models of the urine concentrating mechanism. Investigation of intra-renal solute distribution, and its cycling by way of countercurrent exchange and preferential tubular interactions, may yield new insights into fundamental principles of concentrating mechanism function. Our method is implemented in a dynamic formulation of a central core model that represents renal tubules in both the cortex and the medulla. Axial solute diffusion is represented in intratubular flows and in the central core. By representing the fate of solute originally belonging to a marked bolus, we obtain the distribution of that solute as a function of time. In addition, we characterize the residence time of that solute by computing the portion of that solute remaining in the model system as a function of time. Because precise mass conservation is of particular importance in solute tracking, our numerical approach is based on the second-order Godunov method, which, by construction, is mass-conserving and accurately represents steep gradients and discontinuities in solute concentrations and tubular properties.

*Keywords:* Kidney; mathematical model; Godunov method.

### 1. Introduction

To maintain a steady blood plasma osmolality, mammals are capable of producing a urine with a much higher osmolality than that of blood plasma during periods of water deprivation. This regulation of blood plasma osmolality is provided by the kidney's urine concentrating mechanism, which is localized in the renal medulla. In the outer medulla, the concentrating mechanism is driven by active NaCl transport from thick ascending limbs. This concentrating effect, coupled with a countercurrent flow configuration of tubules and vessels, generates an osmolality gradient along all structures of the outer medulla, from the cortico-medullary boundary to the outer-inner medullary boundary. In contrast, the underlying mechanism in the inner medulla remains one of the long-standing mysteries in traditional physiology, despite much experimental and modeling effort.

Investigation of intra-renal solute distribution, and its cycling by way of counter-current exchange and preferential tubular interactions, allows model predictions to be compared with micropuncture data and with solute cycling paths inferred from anatomy and permeability data. Thus, such investigation may yield new insights into fundamental principles of urine concentrating mechanism function. In [19], Thomas gave an extensive quantitative analysis of net steady-state transmural fluxes and predicted solute and water cycling patterns, using a model that represents detailed radial organization of medullary structures and captures their preferential interactions [21].

Models of the urine concentrating mechanism, such as [21] mentioned above, have usually been formulated as steady-state boundary-value problems involving differential equations expressing solute and water conservation. Solute and water cycling patterns are predicted via an examination of steady-state model solutions, as in [19]. In this study, we propose an alternative approach for examining intra-renal solute distribution and cycling: by tracking the dynamic distribution of a marked bolus of solute. (This is similar to tracer experiments in which a small amount of fluid containing a radioactive solute is injected into a renal tubule or a group of tubules.) In contrast to the traditional steady-state approach, our model is formulated in terms of its dynamic equations. We believe that the dynamic model is more intuitive, in part because it can be combined with visualization techniques to generate computer animations of the dynamic distributions of a bolus. Such animations can be used in demonstrations and lectures, and are particularly helpful in answering such questions as “What happens to a solute in the kidney?”

Because mass balance is crucial in tracking filtered solutes, model equations are integrated using a numerical method that is based on the Godunov method [3] and that is mass-conserving by construction. The method is implemented in a dynamic formulation of a central core model that represents renal tubules in both the cortex and the medulla. By computing the fate of solute originally belonging to a marked bolus in the proximal tubule, we obtain the distribution of that solute as a function of time throughout the cortex and medulla. In addition, we characterize the residence time of that solute in the model kidney by computing the portion of that solute remaining in the model as a function of time; residence time provides a measure of the system’s efficacy in trapping that solute.

## 2. Model Formulation

In this section, we introduce the equations for a dynamic, one-loop model of the urine concentrating mechanism for tracking solute distribution. The model, which is based on the central core (CC) formulation [18], represents a single nephron, with a descending limb (DL), an ascending limb (AL), and a collecting duct (CD). These tubules interact in a CC, which represents the vasculature and interstitium. The model configuration is shown in Fig. 1.

The DL, AL, CD, and CC are represented by rigid tubules (indexed by  $i = 1, 2, 3,$

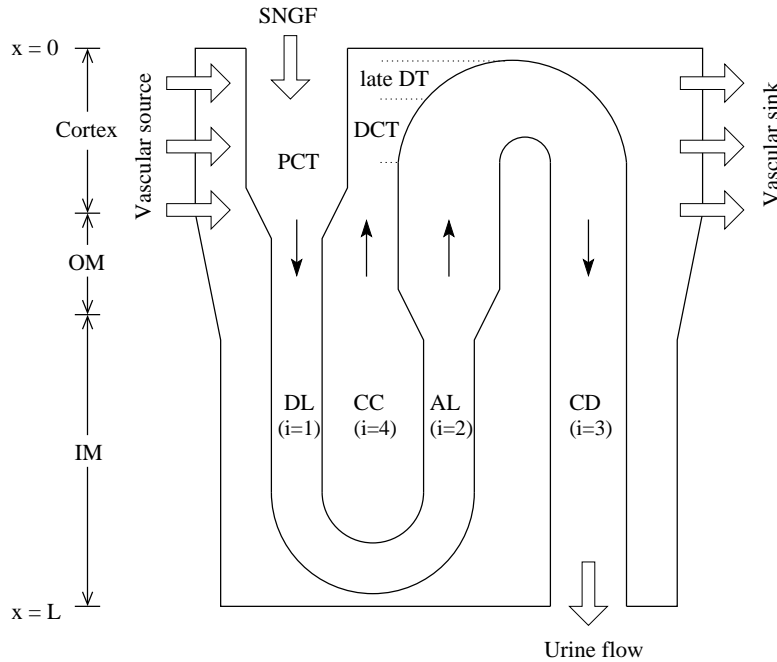


Fig. 1. Model configuration. SNGF, single-nephron glomerular filtration. OM, outer medulla; IM, inner medulla; PCT, proximal convoluted tubule; DL, descending limb; AL, ascending limb; DCT, early distal convoluted tubule; DT, distal tubule; CD, collecting duct; CC, central core. Arrows indicate steady-state flow directions.

and 4, respectively) that extend in space from  $x = 0$  (cortical boundary) to  $x = L$  (papillary tip). Loops of Henle that reach into the papilla likely originate from the juxtamedullary glomeruli (not represented in the model), which are located near the cortico-medullary boundary. However, for simplicity we assume that the DL originates at the cortical boundary ( $x = 0$ ). The cortical segment and the initial outer-medullary segment of the DL correspond to the proximal convoluted tubule (PCT) and the proximal straight tubule (PST), respectively, which, though strictly not part of the DL, we consider them so. Similarly, the model AL also includes the early distal convoluted tubule (DCT), which follows the cortical portion of the thick AL and lies beyond the macula densa (not represented in the model), and the late distal tubule that follows.

The model is formulated for NaCl (represented by  $\text{Na}^+$ ), urea, and a non-reabsorbable solute (denoted by NR and loosely identified as KCl). The model predicts fluid flow, solute concentrations, transtubular water and solute fluxes, and fluid osmolality (arising from NaCl, urea, and NR), as functions of cortico-medullary depth, in the tubules and in the CC. To follow the fate of a marked bolus of a particular solute, we treat the bolus as a distinct solute that has the same transport properties as the original (or, background) solute. Thus, if boluses of  $\text{Na}^+$  and urea

are tracked, five solutes are simulated in the model.

Model equations represent the conservation and transtubular transport of solutes and water. Detailed justification for the model equations can be found in [12]. The water flow rate at time  $t$  in a given tubule  $i$  is denoted by  $F_{iV}(x, t)$ , and the transtubular water line flux (i.e., the water transport rate per unit tubular length) is given by  $J_{iV}(x, t)$ , taken positive for transport into the tubule. With this notation, water conservation is represented in a DL, AL, and CD ( $i = 1, 2$ , and  $3$ ) by

$$\frac{\partial}{\partial x} F_{iV}(x, t) = J_{iV}(x, t) \quad (2.1)$$

Renal arteries enter the renal tissue at the boundary between cortex and medulla, where they eventually give rise to interlobular arteries that supply the cortex through on a radial course. Blood is drained from the cortex by the renal veins. The vascular source and sink are denoted by  $J_{\text{src}}(x)$  and  $J_{\text{sink}}(x, t)$ , respectively. Thus water conservation in the CC is given by

$$\frac{\partial}{\partial x} F_{4V}(x, t) = J_{4V}(x, t) + J_{\text{src}}(x) - J_{\text{sink}}(x, t) \quad (2.2)$$

where in the medulla  $J_{\text{src}}(x) = 0$  and  $J_{\text{sink}}(x, t) = 0$ .  $J_{\text{src}}(x)$  is assumed known a priori, whereas  $J_{\text{sink}}(x, t)$  is determined by assuming that the CC is closed at the cortical boundary, i.e.,  $F_{4V}(0, t) = 0$ , and by assuming that  $J_{\text{sink}}(x, t)$  is uniformly distributed along the cortex. Thus, for  $0 \leq x \leq x_{\text{C-OM}}$ , where  $x_{\text{C-OM}}$  denotes the cortico-medullary boundary,

$$J_{\text{sink}}(x, t) = -\frac{1}{x_{\text{C-OM}}} \left( F_{4V}(x_{\text{C-OM}}, t) - \int_0^{x_{\text{C-OM}}} J_{4V}(x, t) dx \right) \quad (2.3)$$

For a given tubule of type  $i$  and a solute of type  $k$ , let  $C_{ik}(x, t)$  be the solute concentration,  $A_i(x)$  be the cross-sectional area of the tubule,  $D_{ik}$  be the axial diffusion coefficient,  $J_{ik}(x, t)$  be the transtubular solute line flux, taken positive into the tubule, and  $F_{ik}(x, t) \equiv F_{iV}(x, t)C_{ik}(x, t)$  be the solute flow rate. Using this notation, solute conservation is then represented in the DL, AL, and CD by

$$\frac{\partial}{\partial t} C_{ik}(x, t) = \frac{1}{A_i(x)} \left( \frac{\partial}{\partial x} \left( -F_{ik}(x, t) + D_{ik} \frac{\partial C_{ik}}{\partial x} \right) + J_{ik}(x, t) \right) \quad (2.4)$$

Solute conservation in the CC takes into account the vascular source and sink in the cortex:

$$\begin{aligned} \frac{\partial}{\partial t} C_{4k}(x, t) = & \frac{1}{A_4(x)} \left( \frac{\partial}{\partial x} \left( -F_{4k}(x, t) + D_{4k} \frac{\partial C_{4k}}{\partial x} \right) + J_{4k}(x, t) \right. \\ & \left. + J_{\text{src}}(x)C_{\text{VR},k}(x) - J_{\text{sink}}(x, t)C_{4k}(x, t) \right) \end{aligned} \quad (2.5)$$

where  $C_{\text{VR},k}(x)$  denotes the concentration of solute  $k$  in blood plasma.

The transtubular water flux in a DL, AL, or CD is given by

$$J_{iV}(x, t) = 2\pi r_i(x) \bar{V}_w P_{if}(x) \sum_k \phi_k (C_{ik}(x, t) - C_{4k}(x, t)) \quad (2.6)$$

where  $r_i(x)$  is the radius of the tubule,  $\bar{V}_w$  is the partial molar volume of water (0.018136 cm<sup>3</sup>/mmole at 37°C, see p. B-152 and p. F-5 in [20]),  $P_{if}(x)$  is the transtubular osmotic water permeability, and  $\phi_k$  is the osmotic coefficient of solute  $k$ . Reflection coefficient is assumed to be 1 for each solute. For the CC, the equation for transtubular water flux arises from fluxes in (2.6) and is given by

$$J_{4V}(x, t) = -J_{1V}(x, t) - J_{2V}(x, t) - n_{\text{CD}}J_{3V}(x, t) \quad (2.7)$$

where  $n_{\text{CD}}$  is the ratio of the total number of CDs to loops of Henle.

The transtubular solute flux in a DL, AL, or CD is given by

$$J_{ik}(x, t) = 2\pi r_i(x) \left( P_{ik}(x) (C_{4k}(x, t) - C_{ik}(x, t)) - \frac{V_{\text{max}, ik}(x) C_{ik}(x, t)}{K_{M, ik}(x) + C_{ik}(x, t) + C_{ik^*}(x, t)} \right) \quad (2.8)$$

where  $k = (\text{bolus or background}) \text{Na}^+$  or urea. Because all tubules are assumed impermeable to NR,  $J_{i, \text{NR}}(x, t) = 0$ . If  $k$  denotes a background/bolus solute, then  $k^*$  denotes the corresponding bolus/background solute. The first term inside the pair of large parentheses is transtubular diffusion characterized by permeability  $P_{ik}(x)$ . The second term represents active transport, characterized by Michaelis-Menten kinetics with Michaelis constant  $K_{M, ik}(x)$  and maximum transport rate per unit tubular area  $V_{\text{max}, ik}(x)$ ; competition between bolus and background solute for the same transporter is represented. For the CC, the equation for solute flux arises from (2.8) and is given by

$$J_{4k}(x, t) = -J_{1k}(x, t) - J_{2k}(x, t) - n_{\text{CD}}J_{3k}(x, t) \quad (2.9)$$

To complete the system, boundary conditions must be specified. At the entrance of the DL (i.e., the PCT),  $F_{1V}(0, t)$  and  $C_{1k}(0, t)$  for each solute  $k$  must be specified. At the loop bend, the DL is continuous with the AL; thus,  $F_{2V}(L, t) = -F_{1V}(L, t)$ , where the negative sign indicates that flow is taken positive in the increasing  $x$  direction; and for each solute  $k$ ,  $C_{2k}(L, t) = C_{1k}(L, t)$ . At  $x = 0$  a number of late distal tubules empties their content into a CD; thus,  $F_{3V}(0, t) = -F_{2V}(0, t)/n_{\text{CD}}$ , and for each solute  $k$ ,  $C_{3k}(0, t) = C_{2k}(0, t)$ . The CC is assumed to be closed at  $x = L$ , which implies that there is no convective entry of solute or fluid at  $x = L$ ; thus,  $F_{4V}(L, t) = 0$ .

To initialize the model, a steady-state solution is computed for the background solutes only, with bolus solute concentrations set to zero everywhere. Suppose that at time  $t_0$ , a marked bolus of solute  $k$  is injected into the DL at site  $x^*$ . To track the distribution of that bolus, the background solute is replaced by its bolus counterpart (i.e., solute  $k^*$ ) for an infinitesimal time interval; i.e., for  $t \in [t_0, t_0 + \epsilon]$ ,  $C_{1k}(x^*, t) = 0$  and  $C_{1k^*}(x^*, t) = C_{1k}(x^*, t')$ , where  $t' \notin [t_0, t_0 + \epsilon]$  and  $\epsilon > 0$ . The concentration of solute  $k^*$  in time describes the distribution of the bolus.

**2.1. Model parameters**

Model parameters are chosen to approximate a rat kidney in antidiuretic state. Because the goal of this study is to develop a methodology for tracking filtered solute, rather than to develop a sophisticated model of the kidney, many simplifying assumptions have been made in the model. In particular, a single loop is represented, whereas in the rat kidney, loops of Henle forms bends at all levels of the inner medulla, leading to a significantly different loop-to-CD load balance in the papilla. Thus, some model parameters have been adjusted from their experimentally measured value in order for model results to better approximate physiological values. For example, in order to achieve some osmolality gradient in the inner medulla, urea permeabilities of the inner-medullary AL and initial inner medullary DL were reduced from experimental measurements, usually taken to be 14–23 and  $13 \times 10^{-5}$  cm/s [5,6], respectively. Another example is that the maximum active  $\text{Na}^+$  transport rate of thick ALs (6 nmole/(cm<sup>2</sup>s)) was chosen to achieve an osmolality increase of  $\sim 2$  in the outer medulla, whereas experimental data suggests rates of 10.5 and 25.9 nmole/(cm<sup>2</sup>s) in the outer and inner stripes, respectively [2] (based on outer and inner stripe luminal diameters of 21 and 16  $\mu\text{m}$ , respectively).

Table 1. Transtubular transport parameters and diameters. LDT, late distal tubule. Parameters given in the cortex for DL correspond to PCT; and parameters given for AL correspond to LDT in the upper cortex and to AL/DCT in the lower cortex. The vertical line | and arrow  $\rightarrow$  indicate that parameter is assumed to vary abruptly and exponentially, respectively; see text.

			$P_{\text{Na}^+}$	$P_{\text{urea}}$	$P_f$	$V_{\text{max,Na}^+}$	Diameter
			( $10^{-5}$ cm/s)	( $10^{-5}$ cm/s)	( $\mu\text{m/s}$ )	(nmole/(cm <sup>2</sup> s))	( $\mu\text{m}$ )
DL	Cortex	(DL/PCT)	20	1.5	2000	10	80
	OM	(DL/PST)	20	10	2000	0	20
	IM		1	0.1	2000   0	0	20
AL	Cortex	(LDT)	0	1	150	0	80
	Cortex	(AL/DCT)	0	0	0	2	20
	OM		0	0	0	6	20
	IM		80	0.5	0	0	20
CD	Cortex		0.1	0	300	0	20
	OM		0.1	0.5	300	0	20
	IM		0.1	1 $\rightarrow$ 10	500	0	20

We assume a CD-to-loop ratio of  $n_{\text{CD}} = 1/5$ . The lengths of the cortex, outer medulla, and inner medulla are 3, 2, and 5 mm, respectively [7]. Transtubular transport properties and diameters are given in Table 1. The model incorporates recent immunohistochemical evidence that the innermost 60% of the inner-medullary thin

DL lack aquaporin-1 and several urea transporters [14]; these findings suggest that this segment of the DL may be water impermeable and urea impermeable. Thus, in the inner medulla, the model DL is structurally divided into two segments. The first segment, which spans the first 40% of the inner medulla, has high water permeability and low  $\text{Na}^+$  and urea permeabilities; the second segment, which spans most of the rest of the inner medulla, has low  $\text{Na}^+$  and urea permeabilities and is water impermeable. In the cortex, the AL is assumed to be structurally divided into two segments. Near the cortico-medullary boundary is a water-impermeable segment that includes the cortical portion of the thick AL and the early DCT; this segment spans the lower half of the cortex. In the upper half of the cortex the model AL represents the water-permeable late distal tubule that connects to the cortical CD. In the first (upper) half of the inner medulla, the CD is assumed to have a urea permeability (in  $10^{-5}$  cm/s) of  $P_0 = 1$ ; in the second (lower) half of the inner medulla, CD urea permeability increases exponentially to  $P_1 = 10$ , given by

$$P_{3,\text{urea}}(x) = P_0 + (P_1 - P_0) \frac{\exp(10(x - x_{\text{urea}})/L) - 1}{\exp(10(1 - x_{\text{urea}}/L)) - 1} \quad (2.10)$$

for  $x \geq x_{\text{urea}}$ , where  $x_{\text{urea}} = 7.5$  mm.

Cell types are assumed to change abruptly along tubules at the cortico-medullary and outer-inner medullary boundaries, and at the other locations described above. Thus, transport parameters may be discontinuous. Tubules are assumed to have no active urea transport and zero NR permeability, i.e.,  $V_{\text{max},i,\text{urea}} = 0$  and  $P_{i,\text{NR}} = 0$ . The Michaelis constant for active  $\text{Na}^+$  transport is set to 40 mM. The osmotic coefficients  $\phi_k$  were set to be 1.84 for NaCl, 0.97 for urea [20], and 1.84 for NR. Axial diffusion coefficients  $D_{ik}$  are set to be 0.1.

Luminal areas of the PCT and the distal tubule take into account their tortuosity. Because the CDs undergo successive coalescences along the inner medulla, the population of CDs also decreases as a function of increasing medullary depth. In the model, all CDs are merged into a single composite tubule, and the effect of the coalescences is represented by decreasing the tubular radius as a function of increasing medullary depth. That radius is decreased through multiplication by the fraction of CDs remaining at medullary level  $x$ , which is approximated by

$$w_{\text{CD}}(x) = \begin{cases} 1 & x \leq x_{\text{OM-IM}} \\ \exp(-(x - x_{\text{OM-IM}})/(1 - x_{\text{OM-IM}})) & x > x_{\text{OM-IM}} \end{cases} \quad (2.11)$$

where  $x_{\text{OM-IM}}$  denotes the inner-outer medullary boundary. Luminal area of the CC is assumed to equal that of a tubule and is scaled with the CD population in the inner medulla.

At the cortical boundary, the water flow rate and solute concentrations for the PCT are set to  $F_{1V}(0, t) = 30$  nl/min,  $C_{1,\text{Na}^+}(0, t) = 160$  mM,  $C_{1,\text{urea}}(0, t) = 15$  mM, and  $C_{1,\text{NR}}(0, t) = 0.2$  mM. Plasma solute concentrations are assumed to equal those at the entrance of the PCT. The total vascular source in the cortex is assumed to be 9 times the single-nephron filtration rate; thus,  $J_{\text{src}}(x) = 9F_{1V}(0, t)/x_{\text{C-OM}}$ .

### 3. Numerical Method

Because precise mass conservation is of particular importance in solute tracking, our numerical approach is based on the second-order Godunov method [3]. In addition to being mass conservative, Godunov method also accurately represents steep gradients and discontinuities in solute concentrations and tubular properties.

In the numerical discretization, let  $\Delta t$  and  $\Delta x$  denote the time step and spatial grid interval, respectively, such that  $\Delta t > 0$  and  $\Delta x \equiv L/N$ , where  $N$  is the number of spatial grid subintervals. Let  $t_n \equiv n\Delta t$  be the  $n$ th time-level for  $n = 0, 1, \dots$ , and let  $x_j \equiv j\Delta x$  be the  $j$ th spatial grid point for  $j = 0, 1, \dots, N$ . For an arbitrary function  $\psi(x, t)$ , let  $\psi(x_j, t_n)$  be denoted by  $(\psi)_j^n$ . The numerical solution is given as a ‘‘cell average’’ over space interval  $[x_j, x_{j+1}]$  and time interval  $[t_n, t_{n+1}]$ :

$$(\tilde{\psi})_{j+\frac{1}{2}}^{n+\frac{1}{2}} = \frac{1}{\Delta t \Delta x} \int_{t_n}^{t_{n+1}} \int_{x_j}^{x_{j+1}} \psi(x, t) dx dt \quad (3.1)$$

To advance the model solution by one time step, we first compute left and right cell-edge concentration values at  $t_n$  using cell-averaged values:

$$(C_{ik})_{j-}^n = (\tilde{C}_{ik})_{j-\frac{1}{2}}^{n-\frac{1}{2}} + \left( \frac{\Delta x}{2} - \frac{\Delta t}{2} (\delta \tilde{F}_{ik})_{j-\frac{1}{2}}^{n-\frac{1}{2}} \right) (\delta \tilde{C}_{ik})_{j-\frac{1}{2}}^{n-\frac{1}{2}} \quad (3.2)$$

$$(C_{ik})_{j+}^n = (\tilde{C}_{ik})_{j+\frac{1}{2}}^{n+\frac{1}{2}} + \left( -\frac{\Delta x}{2} - \frac{\Delta t}{2} (\delta \tilde{F}_{ik})_{j+\frac{1}{2}}^{n-\frac{1}{2}} \right) (\delta \tilde{C}_{ik})_{j+\frac{1}{2}}^{n-\frac{1}{2}} \quad (3.3)$$

The  $\delta$  operator denotes a finite-difference approximation to  $\partial/\partial x$  with the application of a limiter to preserve monotonicity; this is necessary in order to avoid unphysical oscillations in solutions, which may arise owing to steep gradients and discontinuities in solute concentrations and tubular properties. For an arbitrary function  $\psi(x)$ , let the forward and backward difference operators be denoted by  $(\Delta^+ \tilde{\psi})_{j+\frac{1}{2}} \equiv \tilde{\psi}_{j+\frac{3}{2}} - \tilde{\psi}_{j+\frac{1}{2}}$  and  $(\Delta^- \tilde{\psi})_{j+\frac{1}{2}} \equiv \tilde{\psi}_{j+\frac{1}{2}} - \tilde{\psi}_{j-\frac{1}{2}}$ . Then,

$$(\delta \tilde{\psi})_{j+\frac{1}{2}} \equiv \begin{cases} 0 & \text{if } (\Delta^+ \tilde{\psi})_{j+\frac{1}{2}} (\Delta^- \tilde{\psi})_{j+\frac{1}{2}} < 0 \\ \frac{1}{2\Delta x} \left( (\Delta^+ \tilde{\psi})_{j+\frac{1}{2}} + (\Delta^- \tilde{\psi})_{j+\frac{1}{2}} \right) & \text{otherwise} \end{cases} \quad (3.4)$$

The cell-edge concentrations are then used to update transtubular water fluxes using (2.6) and (2.7) and transtubular solute fluxes using (2.8) and (2.9). Then intratubular water flows are computed by integrating (2.1) and (2.2) by means of

the trapezoidal rule:

$$(F_{1V})_j^n = (F_{1V})_0^n + \frac{\Delta x}{2} \sum_{l=1}^j \left( (J_{1V})_{l-1+}^n + (J_{1V})_{l-}^n \right) \quad (3.5)$$

$$(F_{2V})_j^n = (F_{2V})_N^n - \frac{\Delta x}{2} \sum_{l=N-1}^{j-1} \left( (J_{2V})_{l+}^n + (J_{2V})_{l+1-}^n \right) \quad (3.6)$$

$$(F_{3V})_j^n = (F_{3V})_0^n + \frac{\Delta x}{2} \sum_{l=1}^j \left( (J_{3V})_{l-1+}^n + (J_{3V})_{l-}^n \right) \quad (3.7)$$

$$(F_{4V})_j^n = -\frac{\Delta x}{2} \sum_{l=N-1}^{j-1} \left( (J_{4V})_{l+}^n + (J_{4V})_{l+1-}^n + (J_{\text{src}})_{l+}^n + (J_{\text{src}})_{l+1-}^n - (J_{\text{sink}})_{l+}^n - (J_{\text{sink}})_{l+1-}^n \right) \quad (3.8)$$

where  $(\psi)_{j\pm}^n \equiv \lim_{\epsilon \rightarrow 0^\pm} \psi(x_j + \epsilon, t_n)$ . Left- and right-limit values are used for the fluxes because of discontinuities in tubular properties.

Then  $(\tilde{C}_{ik})_{j+\frac{1}{2}}^{n+\frac{1}{2}}$  is updated using the advective solute flux  $((F_{ik})_{j-}^n - (F_{ik})_{j+1+}^n)/\Delta x$ , transtubular solute flux  $(J_{ik})_{j+\frac{1}{2}}^n$ , and axial diffusive flux  $((F_{Dik})_{j-}^n - (F_{Dik})_{j+1+}^n)/\Delta x$ , where  $(F_{Dik})_j^n \equiv D_{ik} \partial(C_{ik})_j^n / \partial x$ . The discretized solute conservation equation (2.4) for the DL, AL, and CD is given by

$$\begin{aligned} (\tilde{C}_{ik})_{j+\frac{1}{2}}^{n+\frac{1}{2}} &= (\tilde{C}_{ik})_{j+\frac{1}{2}}^{n-\frac{1}{2}} + \frac{\Delta t}{(A_i)_{j+\frac{1}{2}}} \left( \frac{1}{\Delta x} \left( (F_{ik})_{j+}^n - (F_{ik})_{j+1-}^n \right) \right. \\ &\quad \left. + (F_{Dik})_{j+}^n - (F_{Dik})_{j+1-}^n + (J_{ik})_{j+\frac{1}{2}}^n \right) \end{aligned} \quad (3.9)$$

The cell-centered solute flux  $(J_{ik})_{j+\frac{1}{2}}^n$  is approximated to second order by averaging the left and right cell-edge solute fluxes:  $\frac{1}{2}((J_{ik})_{j+}^n + (J_{ik})_{j+1-}^n)$ . For the CC, fluxes arising from the vascular source and sink must be taken into account:

$$\begin{aligned} (\tilde{C}_{4k})_{j+\frac{1}{2}}^{n+\frac{1}{2}} &= (\tilde{C}_{4k})_{j+\frac{1}{2}}^{n-\frac{1}{2}} + \frac{\Delta t}{(A_4)_{j+\frac{1}{2}}} \left( \frac{1}{\Delta x} \left( (F_{4k})_{j+}^n - (F_{4k})_{j+1-}^n + (F_{D4k})_{j+}^n - (F_{D4k})_{j+1-}^n \right) \right. \\ &\quad \left. + (J_{4k})_{j+\frac{1}{2}}^n + (J_{\text{src}})_{j+\frac{1}{2}}^n (C_{\text{VR}})_{j+\frac{1}{2}}^n - (J_{\text{sink}})_{j+\frac{1}{2}}^n (C_{4k})_{j+\frac{1}{2}}^n \right) \end{aligned} \quad (3.10)$$

#### 4. Numerical Results

In this section, we first present steady-state model solutions computed using the parameters given in Section 2.1. We then present representative time-dependent solutions for a bolus of  $\text{Na}^+$  and of urea, and we characterize the residence times and excretion rates of those solutes. All calculations reported below were performed using Fortran programs executed in double precision on a computer with two Intel Pentium IV 1.8 GHz processors and 1G of RAM. A spatial resolution of  $N = 400$  and a time step of  $\Delta t = 0.0392699$  s were used.

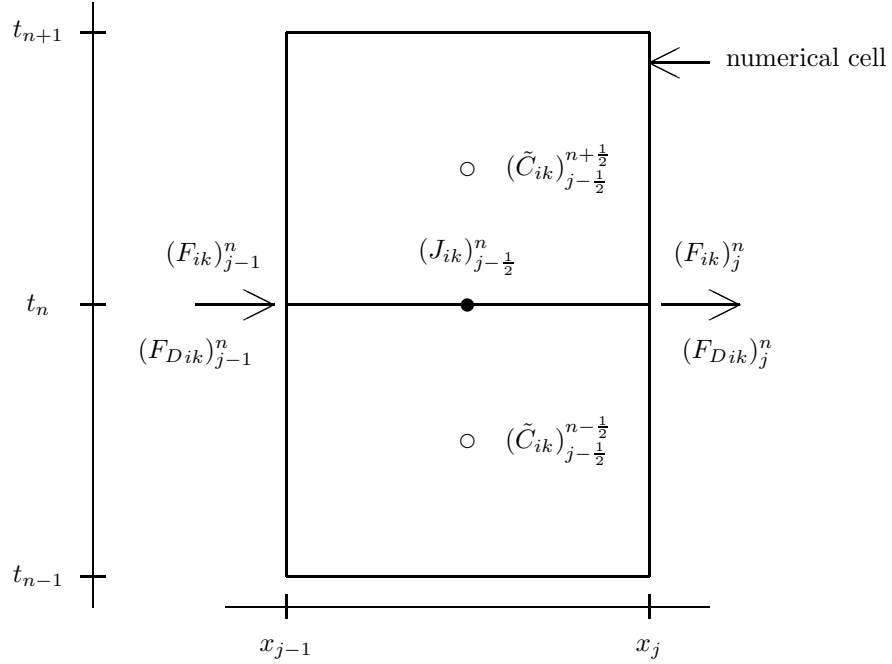


Fig. 2. The Godunov method updates cell-averaged solute concentrations using cell-edge values of solute fluxes. Advective solute flux and axial diffusive flux are shown across cell walls; for the CC, vascular fluxes must also be taken into account.

#### 4.1. *Steady-state solution*

Steady-state  $\text{Na}^+$  concentrations, urea concentrations, osmolality (arising from  $\text{Na}^+$ , urea, and NR) profiles, and water flow rates are shown in Fig. 3. Physiological experiments have shown that the average osmolality of fluid throughout the cortex is near that of plasma osmolality, whereas the average osmolality of fluid at a given medullary level increases monotonically from the cortico-medullary boundary to the papillary tip [4]. Our simulation results show that, in the cortex,  $\text{Na}^+$  and urea concentrations, and thus fluid osmolalities, in the PCT and CC are near that of blood plasma. This is attributable to the large vascular source flow rate, compared to tubular flow rates, at plasma composition in the cortex, with which the highly water-permeable PCT rapidly equilibrates.  $\text{Na}^+$  concentration of the AL fluid mostly decreases along its flow direction, owing to its active, outward-directed transepithelial transport of  $\text{NaCl}$ . Along the late distal tubule, urea concentration increases along the flow direction, owing to water reabsorption.

An increasing osmolality gradient is obtained along the cortico-medullary axis in the outer medulla in all tubules. The average fluid osmolality increases by a factor of  $\sim 2.2$ , a result that is consistent with many model studies [11,16]. The osmolality

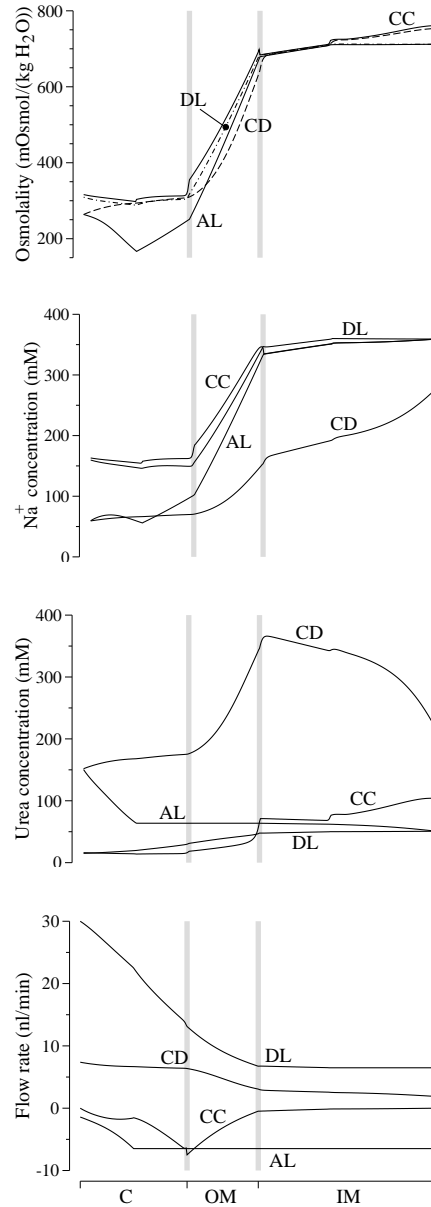


Fig. 3. Steady-state osmolality, Na<sup>+</sup> concentration, urea concentration profiles, and water flow rate. C, cortex; DL. Gray lines indicate C-OM and OM-IM boundaries. Flow is taken positive in the increasing  $x$  direction.

gradient is maintained by active, outward-directed transepithelial transport of NaCl by thick ALs; thus, Na<sup>+</sup> concentration and thus osmolality of the intratubular fluid in the thick AL is progressively reduced along the flow direction. Urea concentration

remains constant because the outer-medullary thick AL is impermeable to both water and urea.

Layton et al. have shown that, in the inner medulla, the water-impermeable papillary segments of DLs and the low NaCl permeability of DLs favor the targeted delivery of NaCl to loop bends, where a favorable transtubular gradient, sustained by urea absorption from CDs, promotes NaCl absorption [10]. Their model predicts an osmolality increase of a factor of  $\sim 2$  in the inner medulla, consistent with a rat in a moderate antidiuretic state [15]. However, in our model, an osmolality increase of 17% was obtained, even though urea permeabilities of thin AL and initial inner medullary DL were reduced from experimental measurements (see Section 2.1; low urea permeabilities are believed to be favorable for generating an inner-medullary osmolality gradient by way of a passive mechanism [11]). This is attributable largely to the single-loop configuration used in this model. As demonstrated in [10], the exponentially decreasing loop population in the inner medulla is critical in balancing the loads between loops of Henle and CDs. (Recall that the CDs undergo successive coalescences in the inner medulla.) By representing only a single loop, even a moderate osmolality increase in the inner medulla is difficult to achieve, unless urea permeabilities of both inner-medullary DL and AL are set to zero.

In the inner medulla, our model predicts that urea is absorbed from the CD, because of the large urea concentration transtubular gradient, which is maintained, in part, by the low CD urea permeability ( $0.1 \times 10^{-5}$  cm/s) in the cortex and outer medulla.  $\text{Na}^+$  is secreted into the CD, which has a relatively low  $\text{Na}^+$  concentration, owing to the vigorous outward-directed  $\text{Na}^+$  active transport along the thick ALs, which then empty their fluid into the CD. In comparison, solute concentrations along the DL and AL change little. For urea, this is attributable to their low permeabilities; for  $\text{Na}^+$ , this is attributed to the failure of the model to generate a substantial transtubular gradient in favor of  $\text{Na}^+$  absorption.

In the DL,  $\sim 77\%$  of the filtered volume is reabsorbed along the PCT, PST, and the outer-medullary portion of the DL. In the inner medulla, little water is reabsorbed from or secreted into the DL because, fluid osmolalities in the DL and CC differ little along the initial 40%, and because the remainder of the DL is water impermeable. Except for the late distal tubule, the AL is water impermeable; thus, water flow rate is constant along most of the AL. Along the late distal tubule,  $\sim 78\%$  of the water is reabsorbed, even though water permeability is low ( $150 \mu\text{m/s}$ ). This is attributable to the low fluid osmolality in the late distal tubule, compared to the CC, generated by the outward-directed active  $\text{Na}^+$  transport of the thick AL. The late distal tubule is contiguous with the cortical CD. Because five late distal tubules are assumed to empty their content into one CD (recall that the CD-to-loop ratio is 1/5), at  $x = 0$  the CD tubular flow is five times that of a late distal tubule. Because this model fails to generate a substantial osmolality gradient in the inner medulla, urine flow rate is predicted to be 0.37 nl/min per nephron (or, per loop of Henle), which is substantially higher than that of a rat in antidiuretic state, reported in one study to be 0.06 nl/min per nephron, based on 38,000 nephrons per kidney [15].

#### 4.2. Bolus distributions

We describe the fate of a bolus that is injected into the DL at the cortico-medullary boundary. To compute the distribution of that bolus, background solutes are first initialized to the steady-state concentrations described in Section 4.1. Then for one timestep, background  $\text{Na}^+$  or urea is replaced by its bolus counterpart for  $x \in [x_{\text{C-OM}}, x_{\text{C-OM}} + 2\Delta x]$ ; bolus solute concentrations are zero everywhere else. By integrating model equations (2.4), (2.5), (2.8), and (2.9), one can track the distribution of the bolus. Because a bolus merely replaces a background solute, fluid osmolalities are not affected. Thus, water flux  $J_{iV}$  and water flow rate  $F_{iV}$  are set to their steady-state values.

Before discussing model results, it is helpful to compute steady-state transit time for each tubule, which suggests where a bolus may be found at a given time. The transit time from the site of bolus entry to loop bend, computed as

$$T_{\text{DL}} = \frac{L - x_{\text{C-OM}}}{\int_{x_{\text{C-OM}}}^L F_{1V}(x, \infty)/A_1(x) dx} \quad (4.1)$$

is 19 s, where  $F_{1V}(x, \infty)$  denotes steady-state DL water flow rate at  $x$ . Transit times for the entire AL (AL and distal tubule) and CD (i.e., from  $x = 0$  to  $x = L$ ) are 550 and 41 s, respectively. Transit time is large for the AL because of the large cross-sectional area and small flow rate in the distal tubule (see Table 1 and Fig. 3). Thus, the total transit time for a bolus of volume, given by  $T_{\text{DL}} + T_{\text{AL}} + T_{\text{CD}}$ , is  $\sim 610$  s.

Figure 4 shows the distribution of a  $\text{Na}^+$  bolus at initial time  $t = 0$ , and after 10 and 600 s. At  $t = 0$ ,  $\text{Na}^+$  bolus concentration was set to be 155 mM, which is the steady-state  $\text{Na}^+$  concentration of the DL fluid at the cortico-medullary boundary. After 15 s, the bolus was near the loop bend, with its peak having lost  $\sim 96\%$  of its magnitude, owing to diffusion, both axial and transtubular. A small hump was observed in the CC bolus concentration in the outer medulla, where DL  $\text{Na}^+$  permeability is significant ( $20 \times 10^{-5}$  cm/s). In contrast, CC bolus concentration is close to 0 in the inner medulla, where DL  $\text{Na}^+$  permeability is low ( $1 \times 10^{-5}$  cm/s). Little of the bolus was found in the CD, owing to its low  $\text{Na}^+$  permeability ( $0.1 \times 10^{-5}$  cm/s). Little of the bolus was found in the AL, because it is  $\text{Na}^+$  impermeable in the outer medulla and because CC bolus concentration is low in the inner medulla. After 600 s, the majority of the bolus was found in the CD. At this time, the peak of the bolus had only  $\sim 0.10\%$  of its initial amplitude. Because of exchanges via the CC and because of axial diffusion, the bolus was distributed among all tubules.

Figure 5 shows the distribution of a urea bolus at initial time  $t = 0$ , and after 15 and 600 s. At  $t = 0$ , urea bolus concentration was set to be  $\sim 31$  mM, the urea concentration of the DL fluid at the cortico-medullary boundary. After 15 and 600 s, the maximum amplitudes of the bolus concentration were  $\sim 9.4\%$  and  $0.14\%$ , respectively, of its original value. After 600 s, the maximum urea bolus concentration

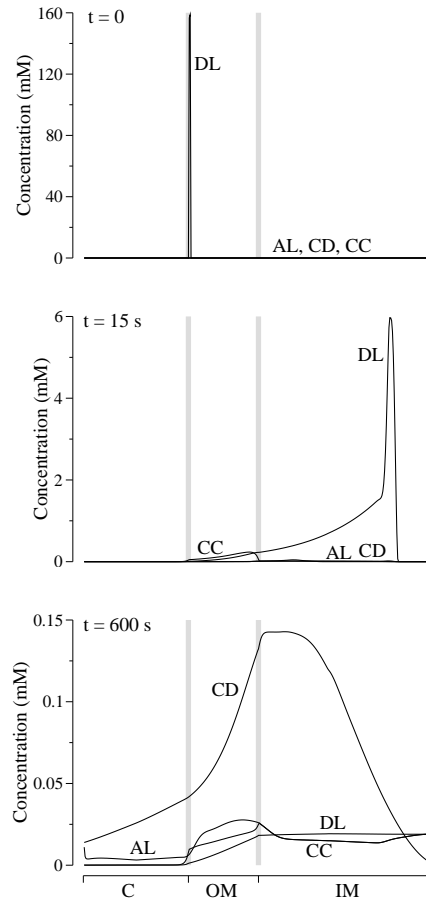


Fig. 4.  $\text{Na}^+$  bolus concentration profiles at  $t = 0, 15,$  and  $600$  s.

in the CD is higher than the  $\text{Na}^+$  bolus, because in most segments of the loop of Henle, urea permeabilities are lower than  $\text{Na}^+$  permeabilities, leading to smaller transtubular urea diffusion.

Model results can also be visualized using computer graphics techniques. Snapshots of an animation of the fate of a urea bolus at  $t = 15$  and  $600$  s are shown in Figs. 6 and 7. The actual animation contains a sequence of such figures. In Fig. 6, both steady-state (red) and bolus (blue) urea concentrations are shown. Steady-state urea concentration is shown in linear scale, where deeper red corresponds to a higher urea concentration. Because bolus concentration varies widely in time, it is shown in a logarithmic scale. To more clearly show the bolus distribution, steady-state solute concentrations can be omitted, as in Fig. 7.

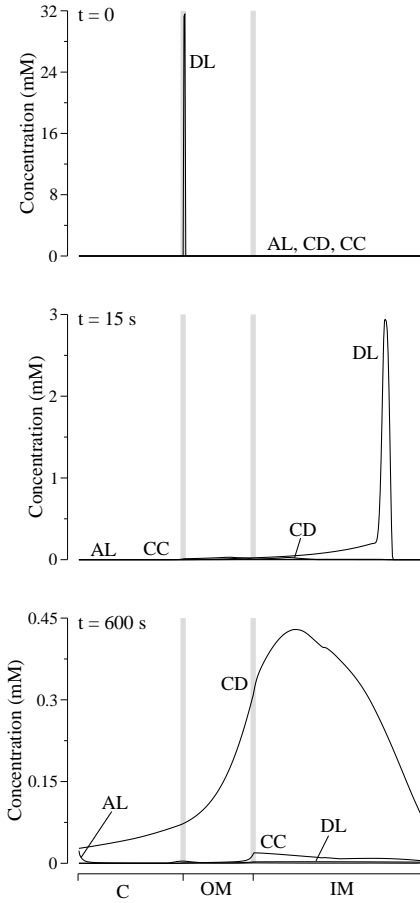


Fig. 5. Urea bolus concentration profiles at  $t = 0$ , 15, and 600 s.

#### 4.3. Residence times and excretion rates

The fraction of solute  $k$  bolus remaining in the system at time  $t$  is given by the ratio of the total amount of bolus remaining and the size of the bolus at initial time  $t = 0$ ; i.e.,

$$f_k(t) = \frac{\int_0^L \left( n_{CD} A_3(x) C_{3k}(x, t) + \sum_{i=1,2,4} A_i(x) C_{ik}(x, t) \right) dx}{\int_0^L A_1(x) C_{1k}(x, 0) dx} \quad (4.2)$$

with the assumption that the bolus was injected at  $t = 0$ .

Fractions of  $\text{Na}^+$  and urea boluses remaining in the system are given in Fig. 8 as functions of time. After injection of a bolus ( $\text{Na}^+$  or urea) at  $t = 0$ , a substantial portion ( $\sim 30\%$ ) of it rapidly disappears when that part of the bolus diffuses from the DL into the CC, advects “upward” into the cortex, and is then drained by the vasculature sink.

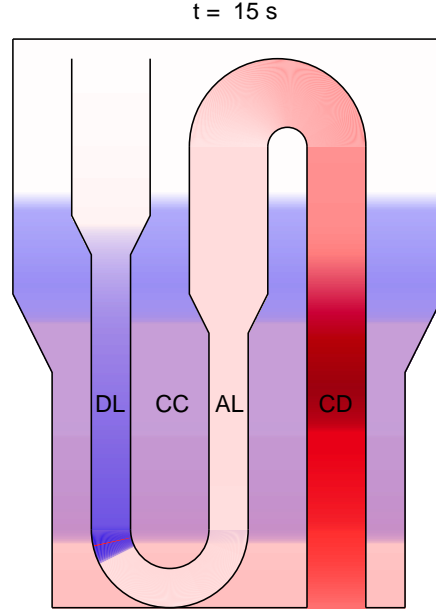


Fig. 6. Distribution of a urea bolus at  $t = 15$  s. Red, steady-state urea concentration in linear scale. Blue, urea bolus concentration in logarithmic scale. Red bar, advected marker originally at front of bolus.

The “half-lives” of  $\text{Na}^+$  and urea (i.e.,  $t$  such that  $f_k(t) = 0.5$ ) are  $\sim 377$  and  $\sim 486$  s, respectively. For 90% of the bolus to disappear, it takes for  $\text{Na}^+$  and urea  $\sim 1130$  and  $\sim 1186$  s, respectively. Recall that the total fluid transit time along the nephron, from the site of bolus injection to the CD at the papillary tip, is  $\sim 610$  s. Thus, much of a bolus does not travel through the entire nephron; instead, it leaves the system either through the cortical vasculature sink as noted above, or through a short-cut—by diffusing from the loop of Henle into the CC, then into the CD and eventually excreted in the urine.

Fractional rates of  $\text{Na}^+$  and urea bolus excretion in urine, given by

$$r_k(t) = \frac{n_{\text{CD}} F_{3V}(L, t) C_{3k}(L, t)}{\int_0^L A_1(x) C_{1k}(x, 0) dx} \quad (4.3)$$

are shown in Fig. 9, top panel. Because the transit time along the DL from the cortico-medullary boundary (site of bolus injection) to  $x = L$  is  $\sim 19$  s, and because water flow rate is higher in the DL than in the CD,  $r_k(t) = 0$  for approximately the first 19 s. The first local maximum for both solutes occurs at  $t = 34$  s, shortly after the bolus enters the AL, which has a higher  $\text{Na}^+$  permeability than DL. At this time, the bolus diffuses through the CC into the CD, and is then excreted in urine. The global maxima for both solutes occur at approximately the total transit

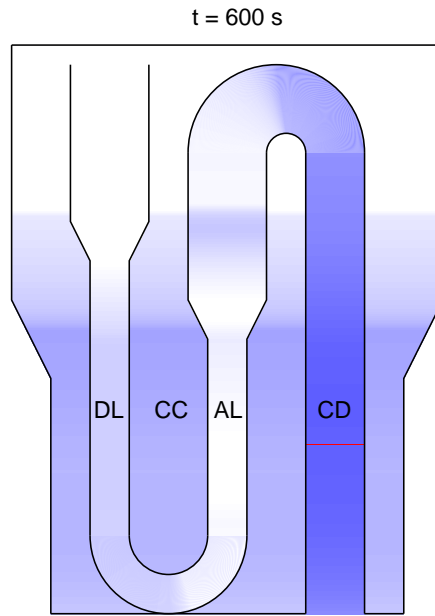


Fig. 7. Distribution of a urea bolus at  $t = 600$  s. Notation is analogous to that used in Fig. 6. Steady-state urea concentration is not shown.

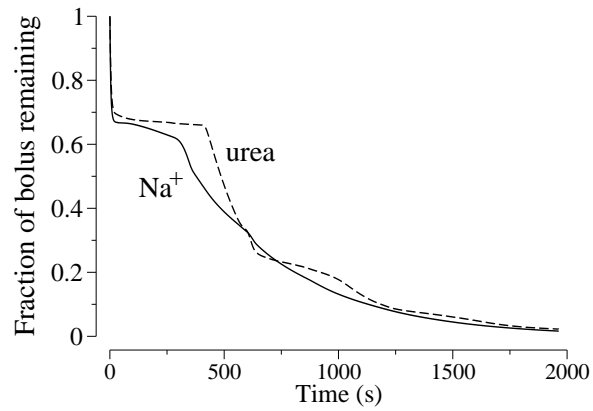


Fig. 8. Fractions of  $\text{Na}^+$  and urea boluses remaining in system as functions of time.

time ( $t = 610$  s).

The fraction of solute  $k$  bolus excreted in urine as a function of time, given by

$$u_k(t) = \int_0^t r_k(s) ds \quad (4.4)$$

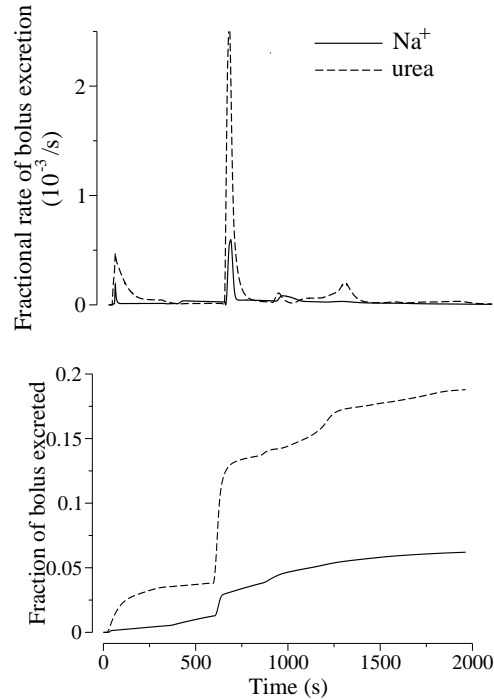


Fig. 9. Top panel: fractional rates of  $\text{Na}^+$  and urea bolus excretion in urine. Bottom panel: fractions of  $\text{Na}^+$  and urea boluses excreted in urine as functions of time.

is shown in Fig. 9, bottom panel. Both curves have a steep increase at approximately the total transit time. At  $t = 2000$  s, 6.2% of the  $\text{Na}^+$  bolus and 19% of the urea bolus has been excreted in urine. At that time, only 16% of the  $\text{Na}^+$  bolus and 22% of the urea bolus remains in the system (see Fig. 8), thus 78% and 59% of the  $\text{Na}^+$  and urea boluses, respectively, are drained via the vasculature sink, which is the only other exit from the system. More  $\text{Na}^+$  than urea is drained via the vasculature sink owing to the active  $\text{Na}^+$  transport of the thick AL.

## 5. Discussion

We have developed a methodology for predicting the time-dependent distributions and residence times of filtered solutes in a mathematical model of the rat urine concentrating mechanism. This is the first urine concentrating mechanism model that focuses on dynamic solutions. The model is based on the CC formulation, and represents a single nephron in the renal cortex and medulla. The numerical method for computing model solutions is based on the second-order Godunov method, which is mass-conserving by construction.

Shortly after its addition, a significant fraction of the bolus is lost via the cortical vasculature sink. The bolus continues to be lost by diffusing into the CC, and

then into the CD to be excreted in urine, or by advecting into the cortex to be drained by the vasculature. Solute exchange via the CC gives rise to multiple extrema in bolus excretion rates in urine. Indeed, most of the bolus does not traverse through the entire nephron (which, of course, would have been the case were tubular permeabilities and active transport rate for that solute set to zero or very low).

One application of the present methodology is the visualization of model results. As demonstrated in Section 4.2, the model can be used to generate computer animations that track the distribution of a bolus. Moreover, one can generate animations to illustrate the evolution of the system to its steady state by omitting the bolus, initializing the system from an arbitrary set of solute concentrations, and integrating the model equations. These animations are suitable for demonstrative purposes or as an educational tool. (Indeed, in the current implementation where bolus concentrations are shown in logarithmic scale, the animations should not be taken as precise representation of model solutions.)

The cycling, or trapping, of solutes by way of countercurrent exchange and preferential tubular interactions is considered an important aspect of the mammalian urine concentrating mechanism. Traditionally, solute cycling has been assessed in a model using the predicted steady-state transmural fluxes or solute flows. The residence time of a bolus provides an alternative, and perhaps more intuitive, measure of the ability of a concentrating mechanism to cycle or trap a solute.

Because the focus of this study is on the development of a numerical methodology, the model is based on the simple CC formulation. The CC formulation does not explicitly represent vasa recta or the radial organization of tubules and vasa recta, both of which are believed to have a significant impact on intra-renal solute cycling. Indeed, this model is substantially simpler than the model [21] used by Thomas to predict water and solute cycling patterns [19] (although our representation of the cortex is in greater detail). Nonetheless, our methodology can be extended to more sophisticated models, including those that represent distributed loops of Henle, which more accurately represent the decreasing loop-of-Henle population in the inner medulla; that explicitly represent vasa recta, which are believed to act as countercurrent exchangers to facilitate solute cycling; and that represent the radial organization of medullary structures, which have been revealed in anatomic studies [8] and which are believed to result in preferential interactions among tubules and vasa recta; examples of such models are [9,13,21]. The resulting more physiologically-realistic models can then be used to simulate tracer experiments (e.g., [1,17]), and to investigate intra-renal solute distribution and cycling, which may yield new insights into fundamental principles of concentrating mechanism function. Furthermore, such models can be used to track not only a bolus of solute, but also of water.

### Acknowledgments

The author thanks Professor Harold Layton for his helpful comments. The relation for Michaelis-Menten kinetics with competitive species appeared in an unpublished document by H. Layton.

Portions of this work were presented at Experimental Biology 2003 and have been published in abstract form (*FASEB J.* 17(4): A485, 2003).

This research was supported by the National Science Foundation, grant DMS-0340654.

### References

- [1] RA Danielson and B Schmidt-Nielsen. Recirculation of urea analogs from renal collecting ducts of high- and low-protein-fed rats. *Am J Physiol*, 223(1):130–137, 1972.
- [2] LC Garg, S Mackie, and CC Tischer. Effects of low potassium diet on Na-K-ATPase in rat nephron segments. *Pflügers Arch*, 394:113–117, 1982.
- [3] SK Godunov. A difference method for numerical calculation of discontinuous solutions of the equations of hydrodynamics. *Mat. Sbornik*, 47:271–306, 1959.
- [4] MA Hai and S Thomas. The time-course of changes in renal tissue composition during lysine vasopressin infusion in the rat. *Pflügers Arch*, 310:297–319, 1969.
- [5] M Imai. Function of the thin ascending limb of Henle of rats and hamster perfused in vitro. *Am J Physiol (Renal Fluid Electrolyte Physiol 1)*, 232:F201–F209, 1977.
- [6] M Imai, J Taniguchi, and K Yoshitomi. Transition of permeability properties along the descending limb of long-loop nephron. *Am J Physiol (Renal Fluid Electrolyte Physiol 23)*, 254:F323–F328, 1988.
- [7] MA Knepper, RA Danielson, GM Saidel, and RS Post. Quantitative analysis of renal medullary anatomy in rats and rabbits. *Kidney Int*, 12:313–323, 1977.
- [8] W Kriz and B Kaissling. Structural organization of the mammalian kidney. In *The Kidney: Physiology and Pathophysiology*, pages 587–654, Philadelphia, 2000. Lippincott Williams & Wilkins.
- [9] AT Layton and HE Layton. A mathematical model of the urine concentrating mechanism in the rat outer medulla: I. Model formulation and base-case results. *Am J Physiol Renal Physiol*, submitted, 2003.
- [10] AT Layton, TL Pannabecker, WH Dantzler, and HE Layton. Two modes for concentrating urine in rat inner medulla. *Am J Physiol Renal Physiol*, submitted, 287:F816–F839, 2004.
- [11] HE Layton. Mathematical models of the mammalian urine concentrating mechanism. In *Membrane Transport and Renal Physiology, The IMA Volumes in Mathematics and Its Applications*, volume 129, pages 233–272, New York, 2002. Springer.
- [12] HE Layton and EB Pitman. A dynamic numerical method for models of renal tubules. *Bull Math Bio*, 56(3):547–565, 1994.
- [13] HE Layton, EB Pitman, and MA Knepper. A dynamic numerical method for models of the urine concentrating mechanism. *SIAM J Appl Math*, 55(5):1390–1418, 1995.
- [14] TL Pannabecker, DE Abbott, and WH Dantzler. Three-dimensional functional reconstruction of inner medullary thin limbs of Henle’s loop. *Am J Physiol Renal Physiol*, 286:F38–F45, 2004.
- [15] JP Pennell, FB Lacy, and RL Jamison. An in vivo study of the concentrating process in the descending limb of Henle’s loop. *Kidney Int*, 5:337–347, 1974.
- [16] JM Sands and HE Layton. Urine concentrating mechanism and its regulation. In

- Seldin DW and Giebisch G, editors, *The Kidney: Physiology and Pathophysiology*, pages 1175–1216, Philadelphia, 2000. Lippincott Williams & Wilkins.
- [17] M Silverman, C Whiteside, CJ Lumsden, and H Steinhart. In vivo indicator dilution kinetics of PAH transport on dog kidney. *Am J Physiol (Renal Fluid Electrolyte Physiol 25)*, 256:F255–F265, 1989.
  - [18] JL Stephenson. Central core model of the renal counterflow system. *Kidney Int*, 2:85–94, 1972.
  - [19] SR Thomas. Cycles and separations in a model of the renal medulla. *Am J Physiol (Renal Fluid Electrolyte Physiol 44)*, 275:F671–F690, 1998.
  - [20] RC (ed.) Weast. *CRC Handbook of Chemistry and Physics*. CRC Press, Cleveland, 55 edition, 1974.
  - [21] AS Wexler, RE Kalaba, and DJ Marsh. Three-dimensional anatomy and renal concentrating mechanism. I. Modeling results. *Am J Physiol (Renal Fluid Electrolyte Physiol 29)*, 260:F368–F383, 1991.